Analysis of Cumulus Cloud Updrafts as Observed with 1-Min Resolution Super Rapid Scan GOES Imagery

JOHN R. MECIKALSKI

Atmospheric Science Department, University of Alabama in Huntsville, Huntsville, Alabama

CHRISTOPHER P. JEWETT

Earth Systems Science Center, University of Alabama in Huntsville, Huntsville, Alabama

JASON M. APKE AND LARRY D. CAREY

Atmospheric Science Department, University of Alabama in Huntsville, Huntsville, Alabama

(Manuscript received 3 December 2014, in final form 6 November 2015)

ABSTRACT

A study was undertaken to examine growing cumulus clouds using 1-min time resolution Super Rapid Scan Operations for Geostationary Operational Environmental Satellite-R (GOES-R) (SRSOR) imagery to diagnose in-cloud processes from cloud-top information. SRSOR data were collected using *GOES-14* for events in 2012–14. Use of 1-min resolution SRSOR observations of rapidly changing scenes provides far more insights into cloud processes as compared to when present-day 5–15-min time resolution GOES data are used. For midday times on five days, cloud-top temperatures were cataloged for 71 cumulus clouds as they grew to possess anvils and often overshooting cloud tops, which occurred over 33–152-min time periods. Characteristics of the SRSOR-observed updrafts were examined individually, on a per day basis, and collectively, to reveal unique aspects of updraft behavior, strength, and acceleration as related to the ambient stability profile and cloud-top glaciation. A conclusion is that the 1-min observations capture two specific cumulus cloud growth periods, less rapid cloud growth between the level of free convection and the 0°C isotherm level, followed by more rapid growth shortly after the time of cloud-top glaciation. High correlation is found between estimated vertical motion (w) and the amount of convective available potential energy (CAPE) realized to the cloud-top level as clouds grew, which suggests that updrafts were responding to the local buoyancy quite strongly. Influences of the environmental buoyancy profile shape and evidence of entrainment on cloud growth are also found through these SRSOR data analyses.

1. Introduction

With the advent of so-called Super Rapid Scan Operations for Geostationary Operational Environmental Satellite-R (GOES-R) (SRSOR) datasets, the GOES provides data rates that meet or exceed many other routinely available meteorological observational systems, such as the National Weather Service Weather Surveillance Radar-1988 Dual-Polarimetric (WSR-88DP) and Automated Surface Observing System (ASOS) observations. Super Rapid Scan observations for pre-GOES-R, such as *GOES-14* (and occasionally during science tests of other GOES), are at 1-min time frequency, while those expected from GOES-R will be collected at up to 30-s intervals (Goodman et al. 2012; Schmit et al. 2015). Beyond simple time sequences (i.e., movies), it is hypothesized that these high-time-frequency SRSOR datasets offer a unique ability to describe physical processes connected to rapidly evolving clouds, moisture discontinuities and frontal boundaries, and rapid changes in environmental quantities.

Schmit et al. (2015) overviewed several potential applications of SRSOR observations; from this study, it is clear that considerable information can be obtained from rapidly changing scenes or events, such as growing convective clouds, low clouds and fog, fires, and gravity

Corresponding author address: John R. Mecikalski, Atmospheric Science Department, University of Alabama in Huntsville, National Space Science and Technology Center, 320 Sparkman Dr., Huntsville, AL 35805-1912.
E-mail: johnm@nsstc.uah.edu

DOI: 10.1175/MWR-D-14-00399.1

wave phenomena. Cintineo et al. (2013) briefly examined SRSOR data for three convective storms (see their Figs. 6 and 7), which relates closely to the analysis to follow. SRSOR observations from *GOES-14* have been collected periodically since 2012, with more extensive and continuous collections done during 8–25 May and 14–28 August 2014, and from 18 May to 12 June and 10–22 August 2015. Similarly, 2.5-min resolution data from the Meteosat Second Generation (MSG) Spinning Enhanced Visible and Infrared Imager (SEVIRI) instrument over Europe have also provided unique views of active weather situations, mostly of severe storm development and evolution (Setvák and Müller 2013; Manzato et al. 2015). Despite the initial assessments of the importance of rapid scan observations from geostationary satellites, few studies have yet delved into the quantitative information that these high-frequency data contain, or more importantly, how these data can be examined toward understanding the physical processes being observed. Without such quantification, these data fall short of their potential benefits to systems and algorithms that can be designed to exploit them.

The goal of this study was to quantify specific information within growing cumulus clouds as observed in SRSOR data, expanding on the overview study of Schmit et al. (2015). The study's hypothesis is that use of 1-min resolution SRSOR observations of rapidly changing scenes will provide far more insights into physical cloud processes, as compared to when present-day 5- or 15-min time resolution GOES data are used. With present-day GOES, deep convection as it grows through the troposphere is only observed in two–four frames. Despite this limited cloud-top temperature information, algorithms using ~15-min resolution GOES data have been shown to be useful in forecasting the first-time occurrence of 35-dBZ reflectivity radar returns, the so-called convective initiation (Mecikalski and Bedka 2006; Mecikalski et al. 2015).

For this study 1-min SRSOR observations of growing cumulus clouds were evaluated related to several research questions on what information of in-cloud processes can be obtained by analyzing cloud-top data (as specifically stated in section 2). Time periods on five days in locations that SRSOR observations existed were selected toward addressing the study's goals, with the preference being to collect information on growing cumulus clouds where they were easily observed in otherwise clear skies not obscured by higher clouds. This study aims to address the processes occurring within the updrafts below cloud top that may be described by these data. Specific guiding science questions therefore include the following: What physical processes within growing convective clouds can be observed (or inferred) at 1-min time resolution that cannot be seen at a 5- or 15-min time scale, and how do updrafts change with temporal variations in the prevailing buoyancy profile with altitude? The discussion below helps frame these questions in the context of convective cloud processes. Unlike prior studies that have examined updrafts within clouds using dual-Doppler radar and cloud-resolving models, GOES SRSOR data only allows us to estimate in-cloud processes from cloud-top observations and characteristics. However, despite this limitation, the degree that SRSOR observations can be used to infer in-cloud processes opens up opportunities for using these 1-min data in operational applications and basic research that were not previously available from more routine 5–15-min resolution geostationary satellite fields.

The paper proceeds as follows: section 2 describes the observations used, the background for this research, and the means by which the main datasets were collected and processed, while section 3 presents the results. Section 4 discusses the main results of this study, and section 5 concludes the paper.

2. Data, background and analysis methods

a. SRSOR updrafts and sounding data collection

Table 1 lists dates and times where 1-min and 4-km resolution 10.7-μm IR SRSOR observations were collected for growing convective clouds for this study. These dates and times were chosen from the 2012–14 SRSOR dataset as available through the National Oceanic and Atmospheric Administration (NOAA) Comprehensive Large Array-data Stewardship System (CLASS). Once a location was identified as possessing actively growing convective clouds, an application in the Interactive Data Language (IDL) was developed and used as a means of collecting cloud-top brightness temperature (T_B) data in the 10.7-μm channel every minute. Data were collected for pixels/small locations with cumulus clouds as identified by a human expert, as cumulus clouds evolved from the ''fair weather'' stage to towering cumulus, eventually into larger cumulus (cumulus humilis, mediocris, and congestus) and eventually cumulonimbus (i.e., into a cloud that eventually possessed a new anvil).

All of the SRSOR cloud data obtained with the IDL tool isolated the coldest pixel within a 5 × 5 GOES IR pixel-sized box as a means of ensuring that a main growing and moving updraft was captured in each 1-min image, and to increase the chances that a cumulus cloud

filled an entire 4-km resolution *GOES-14* pixel. The 5 × 5 pixel tracking methodology used here followed that in Lensky and Rosenfeld (2006), and is used to help insure that a continuous cell is tracked over time. A human expert made sure that the 71 cells tracked were separated in space such that there were no concerns with two adjoining cells merging (i.e., all 71 clouds were >5 pixels from each other), since merging cells over small scales (1–2 pixels) would lead to unexpected cloud-top temperature information, especially when a cloud is immature. The updraft dataset contains convective clouds that were tracked for periods of 33–152 min, depending on how rapidly they grew, until they formed an extensive anvil top, or merged with nearby clouds, which resulted in the termination of tracking. Table 1 also shows the number of individual cumulus cloud updrafts sampled per day along with their duration, for a total of 71 updrafts, as well as several parameters of the individual updrafts: the maximum updraft altitude (MDA) per updraft, the temperature difference between the Rapid Refresh (RAP) model 0°C isotherm level and the MDA ("ΔT ZLVL − MDA" in Table 1), along with the vertical motion (w) at the MDA ("peak w"). [These parameters relate to Figs. 5 and 6 with respect to the time of peak observed updraft growth (i.e., peak w), and will be discussed below.] Information on the temperature that glaciation occurred based on the GOES 3.9-μm channel derived reflectance (ref_{39}) is also available every 1 min, as explained below. The T_B when the ref_{39} falls below 9% is also shown in the far-right column of Table 1.

In addition to SRSOR 10.7-μm T_B data, proximity soundings for each individual convective event of temperature, dewpoint temperature, and mixing ratio were collected from 13-km resolution NOAA RAP model 0-h analysis/initialization grids (Benjamin et al. 2009). A RAP model sounding was collected for each cloud updraft analyzed, within two RAP model grid points (26 km) from a cloud in "clear sky" (nonconvectively contaminated in the model) conditions to represent the preconvective environment. From each RAP model sounding, a level of free convection (LFC) was computed. Over the 33–152-min lifetime of each updraft, in the absence of convective storms developing in the RAP model grid cell of a proximity sounding, temperature and moisture changes would be expected to be small given that the time difference between an hourly model sounding and an SRSOR updraft was ≤30 min.

The profiles of RAP temperature and dewpoint temperature were also used to compute the incremental amount of convective available potential energy (CAPE; J kg^{-1}), or δCAPE, or positive buoyancy an updraft was penetrating through (or was available to the updraft) for each 1 min of cloud growth. The bulk CAPE is effectively a "surface-based CAPE" since RAP surface temperature and dewpoint data were used to define the parcel characteristics. An example of a δCAPE segment is shown in Fig. 1, which is defined here as the amount of CAPE within a vertical depth over which a cumulus cloud updraft penetrated in 1 min. The δCAPE values were summed to produce the bulk surface-based CAPE per RAP sounding. For each updraft, 1-min vertical motions w (m s^{-1}) were then computed by simply noting the change in altitude of a cloud every 1 min [i.e., m $(60\text{ s})^{-1}$], assuming that cloud-top T_B is the temperature of a saturated parcel at the cloud top, and that the parcel follows a moist adiabat to originate at the LFC. We use the notation "δw" to denote 1-min estimates of w from SRSOR observations. The former assumption related to T_B is appropriate for optically thick clouds (e.g., cumulus clouds), with multiwavelength optical thicknesses >38 often used to denote convective clouds (Min and Duan 2005; Hong et al. 2007; Young et al. 2012), in which GOES measures a T_B that very closely approximates the actual cloud-top temperature in the absence of significant amounts of water vapor above cloud and/or for clouds that extend above the 0°C level (Adler and Fenn 1979, 1981; Mecikalski et al. 2011). Here, optical thickness would be determined using water absorbing (1.6, 2.1, and 3.7 μm) and nonabsorbing (0.65, 0.86, and 1.24 μm) wavelengths, as observed in channels on instruments like the Moderate Resolution Imaging Spectroradiometer (MODIS) sensors (Hong et al. 2007) or the Visible Infrared Imaging Radiometer Suite (VIIRS).

To accompany Fig. 1, Table 2 provides definitions for δCAPE, δw, and other quantities as discussed below. Note that in the methodology employed herein, the RAP δCAPE and 1-min incremental w estimates (δw) determined from cloud-top T_B changes are somewhat independent datasets, while no information on the model environmental temperature profile was used to determine w. The "response" of an updraft by way of a vertical acceleration should theoretically reflect the amount of instability an updraft has recently moved through (Cotton et al. 2011, 324–331) to the degree that parcel theory is followed. Ideally, environmental soundings from the raob network could be used. However, for this observational study, the location and particularly the timing of the storms required the use of the RAP model soundings for a characteristic depiction of a transient three-dimensional environment. Other methods for estimating w from geostationary satellite observations have been used by Adler and Fenn [1979, their Eq. (1)] and Adler and Fenn [1981, their Eq. (1)] in

TABLE 1. List of cumulus cloud updrafts attributes. See text for description. Here, MDA is "maximum draft altitude," ZLVL is "0°C isotherm level," and "T_B (ref39 < 9%)" is the *GOES-14* brightness temperature when the 3.9-μm channel derived reflectance is less than 9%. All other acronyms are provided in the main document. The boldface values represent the average values of each column per day.

Day		Draft	Time (UTC)	Peak w ($m\,s^{-1}$)	MDA (m)	ΔT ZLVL − MDA (K)	T_B (ref39 < 9%)
20 Aug 2012							
		1	1602–1705	6.6	3575	−9.6	264
CAPE	2228	2	2017–2146	15–2	9985	24.6	243
LFC	2600	3	2017–2157	16.5	4486	−5.5	237
0°C level	4900	4	2017–2155	12.8	8300	18.2	255
RAP EL	14 300	5	1702–1849	14.7	4980	−2.2	254
ave(MDA − ZLVL)	3233	6	1702–1830	8.3	9094	23.1	260
		7	1702–1810	4.7	6417	6.1	264
		8	1702–1839	11.6	9834	28.7	252
		9	1715–1850	7.7	4881	−2.1	264
		10	1749–1859	7.6	5412	1.0	255
		11	1706–1840	7.6	8800	20.8	262
		12	1754–1859	8.8	9149	24.5	253
		13	2106–2201	12.2	11 274	35.8	260
		14	2036–2129	20.3	11 283	36.4	258
		15	2017–2108	16.5	9897	27.9	260
		16	2032–2137	21.3	9977	29.2	260
		17	2017–2134	8.1	9989	30.0	262
		18	2119–2219	8.1	8789	17.3	262
		19	2031–2028	7.1	8652	21.0	255
		20	2051–2150	13.3	8039	12.9	266
		21	2017–2051	13.5	6956	4.7	264
		22	2017–2050	9.6	9152	19.5	265
				11.46	**8133**	**16.5**	**258.0**
20 Aug 2013							
		1	1501–1628	7.5	8820	23.5	260
CAPE	1502	2	1518–1641	8.8	8343	18.4	264
LFC	1350	3	1553–1652	10.7	7008	9.6	270
0°C level	4480	4	1515–1651	5.6	11 251	41.4	270
RAP EL	11 700	5	1650–1808	9.1	10 727	36.0	262
ave(MDA − ZLVL)	4304	6	1606–1804	4.7	11 340	40.7	271
		7	1646–1832	11.4	9370	23.9	278
		8	1716–1839	10.5	5637	0.1	260
		9	1615–1728	9.3	8495	17.1	268
		10	1626–1756	9.4	8672	18.4	271
		11	1633–1821	7.8	11 818	44.1	272
		12	1630–1758	8.6	8998	22.1	278
		13	1604–1822	11.3	8569	17.3	275
		14	1753–1841	15.1	7781	12.5	266
		15	1730–1857	9.0	11 420	42.2	269
		16	1811–1851	9.9	8684	18.4	272
		17	1658–1857	11.1	4739	−3.9	269
		18	1746–1858	18.3	7282	11.1	259
		19	1629–1833	23.2	8346	16.9	275
		20	1654–1830	14.3	8389	20.0	256
				10.78	**8784**	**21.5**	**268.3**
11 May 2014							
		1	1838–1934	17.8	7905	22.9	250
CAPE	2591	2	1830–1958	18.1	4674	1.5	250
LFC	3100	3	1840–2002	21.0	4623	0.0	251
0°C level	4300	4	1845–1941	14.9	6230	9.8	244
RAP EL	12 960	5	1852–2011	24.4	9840	35.3	248
ave(MDA − ZLVL)	2488	6	1904–2010	23.5	7453	14.6	262
				19.95	**6788**	**14.0**	**250.8**

TABLE 1. (*Continued*)

Day		Draft	Time (UTC)	Peak w (m s^{-1})	MDA (m)	ΔT ZLVL − MDA (K)	T_B (ref39 < 9%)
13 May 2014							
		1	1507–1630	8.0	6376	9.0	272
CAPE	2608	2	1626–1803	8.1	9319	31.6	269
LFC	2025	3	1645–1805	6.9	9061	28.4	272
0°C level	4125	4	1637–1829	7.0	6282	7.8	268
RAP EL	13 125	5	1722–1852	8.1	8742	26.9	255
ave(MDA − ZLVL)	4191	6	1616–1815	6.9	7507	18.0	258
		7	1704–1816	5.9	10 248	38.4	257
		8	1756–1858	8.5	7628	17.6	259
		9	1751–1859	7.2	10 680	40.4	233
		10	1634–1859	7.2	6770	11.0	271
		11	1559–1757	9.9	8862	26.9	271
				7.61	**8316**	**23.3**	**262.3**
22 May 2014							
		1	1701–1832	5.5	5297	6.4	259
CAPE	2433	2	1716–1904	9.7	7987	25.9	255
LFC	990	3	1601–1736	6.0	8489	34.5	268
0°C level	3370	4	1601–1655	4.1	5059	10.3	262
RAP EL	11 300	5	1631–1816	4.9	7755	21.7	268
ave(MDA − ZLVL)	3762	6	1649–1809	11.4	7146	24.9	269
		7	1733–1859	5.6	6583	14.6	254
		8	1602–1749	8.1	8606	32.1	269
		9	1648–1753	9.8	4782	2.8	273
		10	1755–1933	11.7	5570	7.8	255
		11	1806–1934	11.1	8643	28.4	258
		12	1718–1950	9.0	9666	35.1	258
				8.08	**7132**	**20.4**	**262.3**

which the time rate of change of T_B divided by a lapse rate (approximately the moist adiabatic lapse rate) is used to estimate w. Although the Adler and Fenn (1979, 1981) methods are useful, it was decided to avoid using an approximate lapse rate, as done in Adler and Fenn (1981) with respect to overshooting cloud tops for convective storms (2.5 K km^{-1}), versus referencing a cloud-top T_B to the temperature of a saturated parcel at cloud top, as described above. Using RAP model temperature profiles to determine updraft altitudes and δCAPE values is done under the assumption that the RAP model environmental temperature profile is similar to the real ambient environment surrounding the specific clouds analyzed.

While numerous previous studies have examined the nature of updraft cores within cumulus clouds and resultant convective storms with respect to bulk environmental CAPE (Bonesteele and Lin 1978; Weisman and Klemp 1982; Barnes 1995; McCaul and Weisman 2001; Geerts et al. 2009; Kirkpatrick et al. 2011, to name a few), the SRSOR data offer an ability to estimate per-level influences of updraft evolution as clouds grow within a profile of environmental instability. It is hypothesized that a Lagrangian response of cumulus cloud updraft growth to the instability profile will be reflected as 1-min rates of updraft acceleration (to δw). CAPE is an integrated quantity, and, therefore, δCAPE should be viewed as a small segment of the entire buoyancy profile (Fig. 1), from a bottom to a top altitude that a parcel moves through in a 1-min time. The entire CAPE within the atmospheric profile becomes apparent as all 1-min δCAPE values are summed as the tropopause or local equilibrium level (EL) is reached. The $\delta(\text{CAPE})^{1/2}$ values are integrated in the following analysis, from an initial updraft altitude to a given cloud-top altitude, as $\sum\delta(\text{CAPE})^{1/2}$. Since $(\text{CAPE})^{1/2}$ is more closely related to w [or to a $w_{\max}$; see Emanuel (1994), their Eq. (6.3.8)], the correlation analyses to follow are made using δw and $[\sum\delta(\text{CAPE})^{1/2}]$.

The final dataset used in this study was GOES ref$_{39}$, which is also available every 1 min in SRSOR; ref$_{39}$ was computed using the methods outline by Lindsey et al. [2006, their Eqs. (1)–(4)]. In the absence of other IR channels on *GOES-14* known to help delineate water from ice clouds (e.g., 8.7 and 12.0 μm; Strabala et al. 1994; Baum et al. 2000), ref$_{39}$ data were used to help infer cloud-top glaciation, whereas reflectance values falling to below 9% when 10.7-μm cloud-top T_Bs are <273 K are highly correlated with the transition of cloud water particles to ice crystals. However, ref$_{39}$

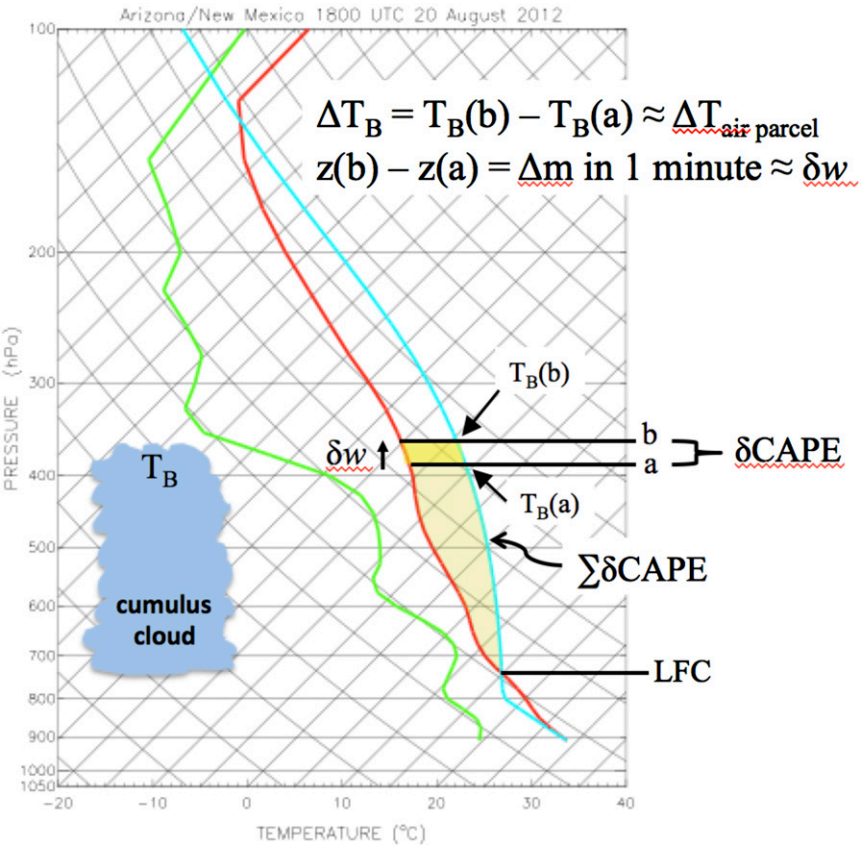

FIG. 1. Schematic showing how δ(CAPE) is estimated with respect to δw, along with several quantities as described in this study. Here, ΔT_B is the cloud-top brightness temperature change estimated from *GOES-14* observations from level a to level b, which is equated to a parcel temperature (blue line) at cloud top ($\Delta T_{\text{air parcel}}$). The δw is the meters per minute (or meters per second) ascent rate of a cumulus cloud, from levels $z(a)$ to $z(b)$ (denoted as Δm), where z is altitude. The δ(CAPE) is the incremental amount of CAPE within a small portion of the entire buoyancy profile [between levels a and b, related to parcel temperatures $T_B(a)$ and $T_B(b)$, respectively] over 1 min of a cloud's vertical ascent. The dark-yellow area represents δ(CAPE). The accumulated CAPE to a given level b is $\sum\delta$(CAPE), and denoted by the larger light-yellow shaded area from the level of free convection (LFC) to level b. See text for further description, and see also Table 2 for definitions of quantities.

values >9% may occur in especially vigorous cumulus cloud updrafts, indicating mixed-phase conditions down to near the homogeneous freezing point of water [Lindsey et al. 2006; see also Rosenfeld and Woodley (2000) and Rosenfeld et al. (2008)]. Therefore, for the results to follow, $\text{ref}_{39} < 9\%$ or 10.7-μm T_B values $\leq$235 K (−38°C) were used to denote glaciation of cloud tops.

b. *Correlation analysis*

Correlations between δw and the summed $\delta(\text{CAPE})^{1/2}$ values $[\sum\delta(\text{CAPE})^{1/2}]$ to a given cloud-top altitude were

TABLE 2. Definitions of terms as used within this paper.

Quantity	Definition
δw (m s^{-1})	1-min vertical motions computed as the change in altitude (m) of a cloud every 1 minute
CAPE (J kg^{-1})	Surface-based convective available potential energy (CAPE) as computed from RAP model profiles of temperature and dewpoint values
δCAPE (J kg^{-1})	The incremental amount of CAPE an updraft penetrated through for each 1 min of cloud growth
$\sum\delta$CAPE (J kg^{-1})	The summed $\delta(\text{CAPE})^{1/2}$ values to a given altitude

computed over 10-min running time segments of all updrafts, from 2 min to $t_{end} - 1$ min, where t_{end} is the ending time of a given analysis period (which varied from 33 to 152 min, as listed in Table 1). These correlations were computed to help assess the correspondence between updraft acceleration rates and the amount of instability within the region a cloud penetrated through within each 10-min period, and will also be used to develop understanding between cloud growth rates and factors influencing B. The 10-min running correlation series help assess whether the measured value of w was behaving in a manner predictable by the amount of CAPE computed through parcel theory. A lack of a correlation between δw and $\sum\delta(\text{CAPE})^{1/2}$ would suggest that the assumptions made with parcel theory have somehow failed to predict SRSOR-estimated values of w, while a high correlation would indicate that there exists a fundamental relationships between satellite-observed cloud ascent rates and local (meso-γ to meso-β scale; 2.5 to ~250 km) instability relevant to the environment within which a cumulus cloud is growing.

c. *Factors influencing parcel vertical accelerations*

The development below is based on parcel theory; however, it has long been recognized that parcel theory is only partially followed near the top of convective clouds, especially in light of entrainment effects (Sloss 1967; Cho 1985; Reuter and Yau 1987), and pressure perturbations due to the presence of buoyancy (Doswell and Markowski 2004). Nevertheless, parcel theory is considered for placing the SRSOR data analysis to follow into the perspective of dynamical processes within convective clouds.

Neglecting dynamic perturbation pressure effects (Emanuel 1994, 6–7), the vertical acceleration of a parcel can be described as follows:

$$\frac{dw}{dt} = -\frac{\rho'}{\rho}g \approx -\frac{T_v'}{\overline{T}_v}g, \tag{1}$$

where g is gravity, ρ is density relative to a hydrostatic basic state, ρ' is the perturbation from the basic state, $\overline{T}_v$ is the basic-state virtual temperature, and T_v' is perturbation virtual temperature. Here, $\rho = \rho_a(1 + q_H)$ is the definition of density given contributions from air (ρ_a) and the hydrometeor mixing ratio (q_H). Equation (1) can be expanded using the equation of state $p = \rho R_d T_v$ and $T_v \approx T(1 + 0.61q_v)$, where q_v is the mixing ratio of water vapor in air (Houze 1993, p. 26 and 36), to give an expression for parcel buoyancy B:

$$B = g\left(\frac{T'}{\overline{T}} - \frac{p'}{\overline{p}} + 0.61q_v - q_H\right). \tag{2}$$

Alternatively, substituting $T_v' = T_v - \overline{T}_v$ in (1), we arrive at an expression for B:

$$\frac{dw}{dt} = -g\frac{(T_v - \overline{T}_v)}{\overline{T}_v} = B. \tag{3}$$

Therefore, by neglecting the effects of pressure perturbations, parcel B has three main contributions that relate back to density perturbations from a basic state, from temperature departures, moisture, and hydrometeor loading. In (2), q_H (“hydrometeor loading”) constitutes a mechanism for decelerating a rising parcel that is otherwise warmer and less dense than its environment.

The 1-min SRSOR data analyzed are available on time scales appropriate to describe rapid accelerations that occur in developing convective clouds, which should be at ~1-min resolution to describe cumuli on horizontal scales of ~2–5 km [Byers and Braham (1949, 17–38); Ludlam and Scorer (1953); see Table 1 in Stechmann and Stevens (2010)]. Many previous studies of convective clouds using satellite observations highlight the significant limitations of lower time resolution (5–15 min) IR ~11-μm “window” and other channel observations for monitoring for convective initiation (Roberts and Rutledge 2003; Sieglaff et al. 2011; Mecikalski et al. 2008, 2011, 2015) and of overshooting cloud tops (Bedka et al. 2010, 2012; Setvák et al. 2013). Therefore, related to (1)–(3) for describing B, and relative to growing convective clouds as observed by SRSOR observations, the guiding research questions stated above (section 1) can be addressed. The following section provides the study’s main results.

3. Results

The results are organized as follows: section 3a focuses on the behavior of individual cumulus cloud growth/updraft cases to help explain the general behavior and patterns seen across the entire dataset, and section 3b presents a statistical analysis of all 71 cases. The 1-min resolution GOES ref_{39} observations coupled to cloud-top T_B measurement are used to help infer the timing of cloud-top glaciation, which is also shown as related to the δw–$\sum\delta(\text{CAPE})^{1/2}$ analyses.

a. *Behavior of individual updrafts*

Figures 2a–e show all SRSOR updrafts for each day analyzed: 20 August 2012 (Fig. 2a), 20 August 2013 (Fig. 2b), 11 May 2014 (Fig. 2c), 13 May 2014 (Fig. 2d), and 22 May 2014 (Fig. 2e). The environmental parameters estimated from the RAP proximity soundings and other characteristics of the updrafts are listed in Table 1 (along

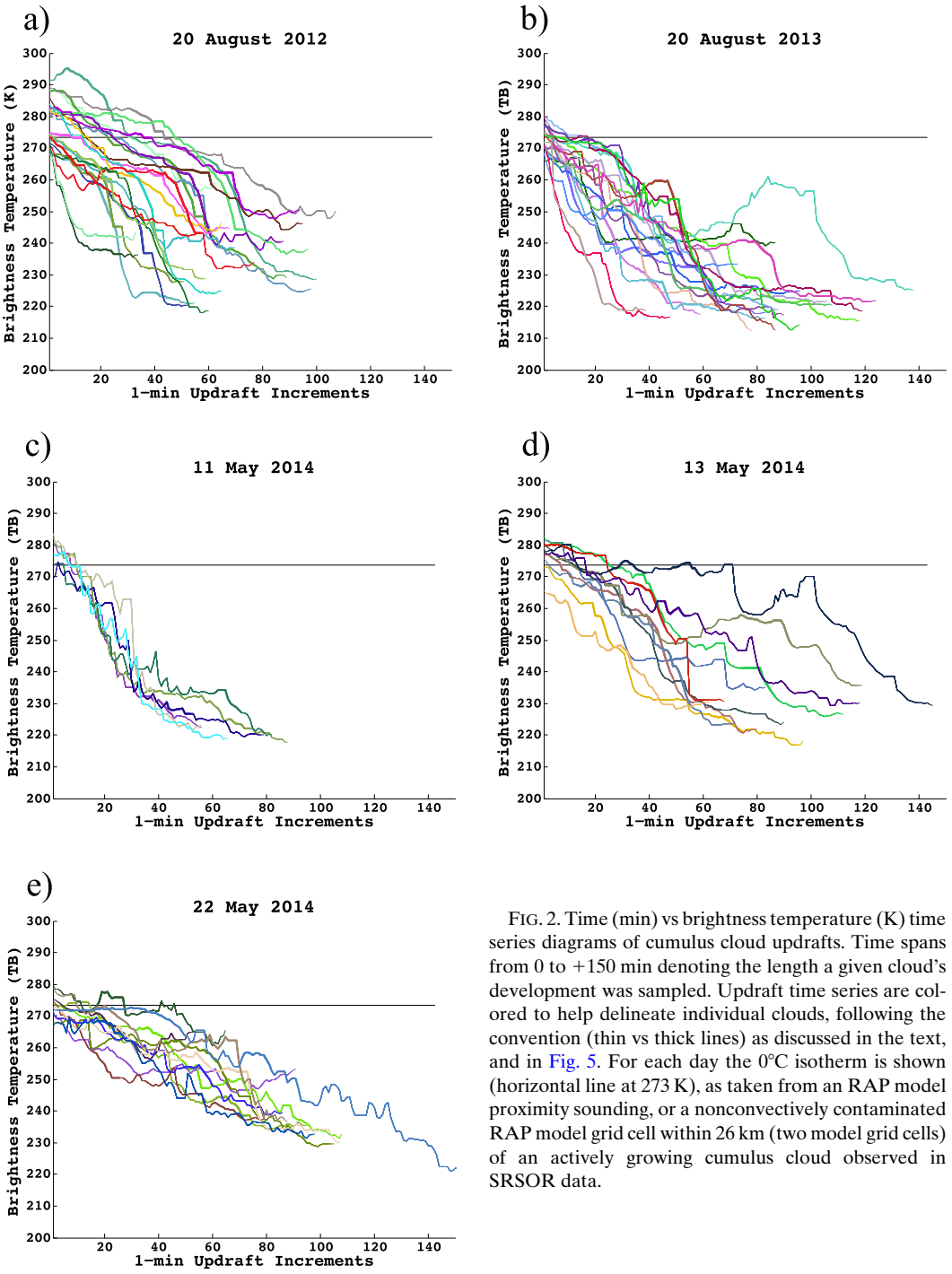

FIG. 2. Time (min) vs brightness temperature (K) time series diagrams of cumulus cloud updrafts. Time spans from 0 to +150 min denoting the length a given cloud's development was sampled. Updraft time series are colored to help delineate individual clouds, following the convention (thin vs thick lines) as discussed in the text, and in Fig. 5. For each day the 0°C isotherm is shown (horizontal line at 273 K), as taken from an RAP model proximity sounding, or a nonconvectively contaminated RAP model grid cell within 26 km (two model grid cells) of an actively growing cumulus cloud observed in SRSOR data.

with the UTC times of each updraft). Shown in Figs. 2a–e are the trends in 10.7-μm cloud-top T_Bs over time. Regions where the correlation between δw within the layer the updraft moved through and $\sum\delta(\text{CAPE})^{1/2}$ are $\geq$0.60 are shown as bolded line segments to demonstrate times when an updraft was apparently responding strongly to the available instability (or more closely following parcel theory). Further discussion of this correlation analysis is provided below, while the 0.60 Pearson correlation coefficient implies a significance of 0.0333 (or a >96.67% chance that the null hypothesis can be rejected) and that there is a significant correlation between the two 10-element datasets δw and $\sum\delta(\text{CAPE})^{1/2}$ (Cohen et al. 2003; Soper 2015). Figures 3a–e show the geographical

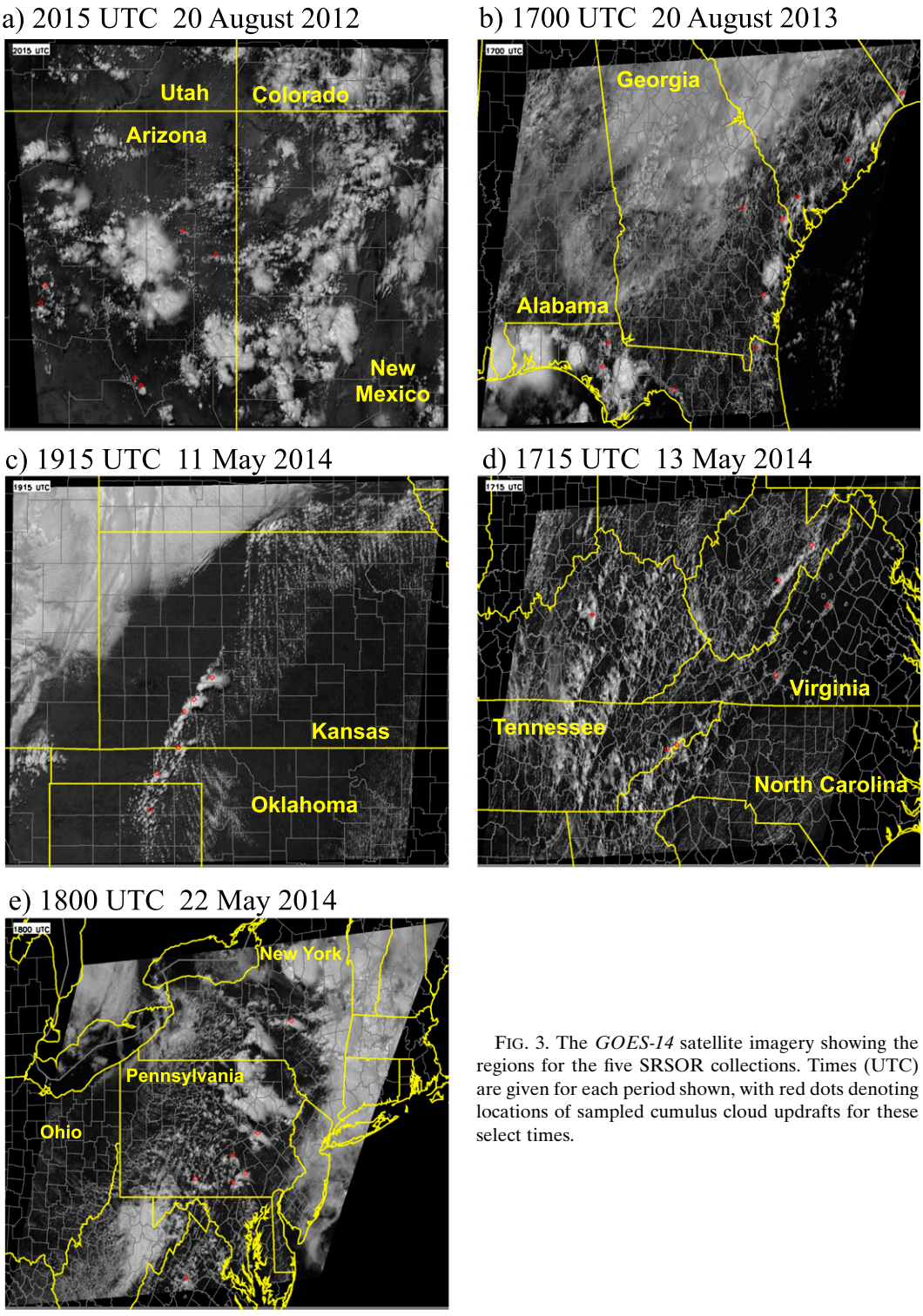

FIG. 3. The *GOES-14* satellite imagery showing the regions for the five SRSOR collections. Times (UTC) are given for each period shown, with red dots denoting locations of sampled cumulus cloud updrafts for these select times.

domains for each date within a sample GOES image, along with several updraft locations (denoted as red dots). Figures 4a–e show a proximity sounding from the RAP model for a time within each day's updraft collection period. For all updraft dates and times, the closest in time RAP sounding was used.

Updrafts on 20 August 2012 (Fig. 2a) were cataloged over a range of initial altitudes from near 2400 to 6500 m

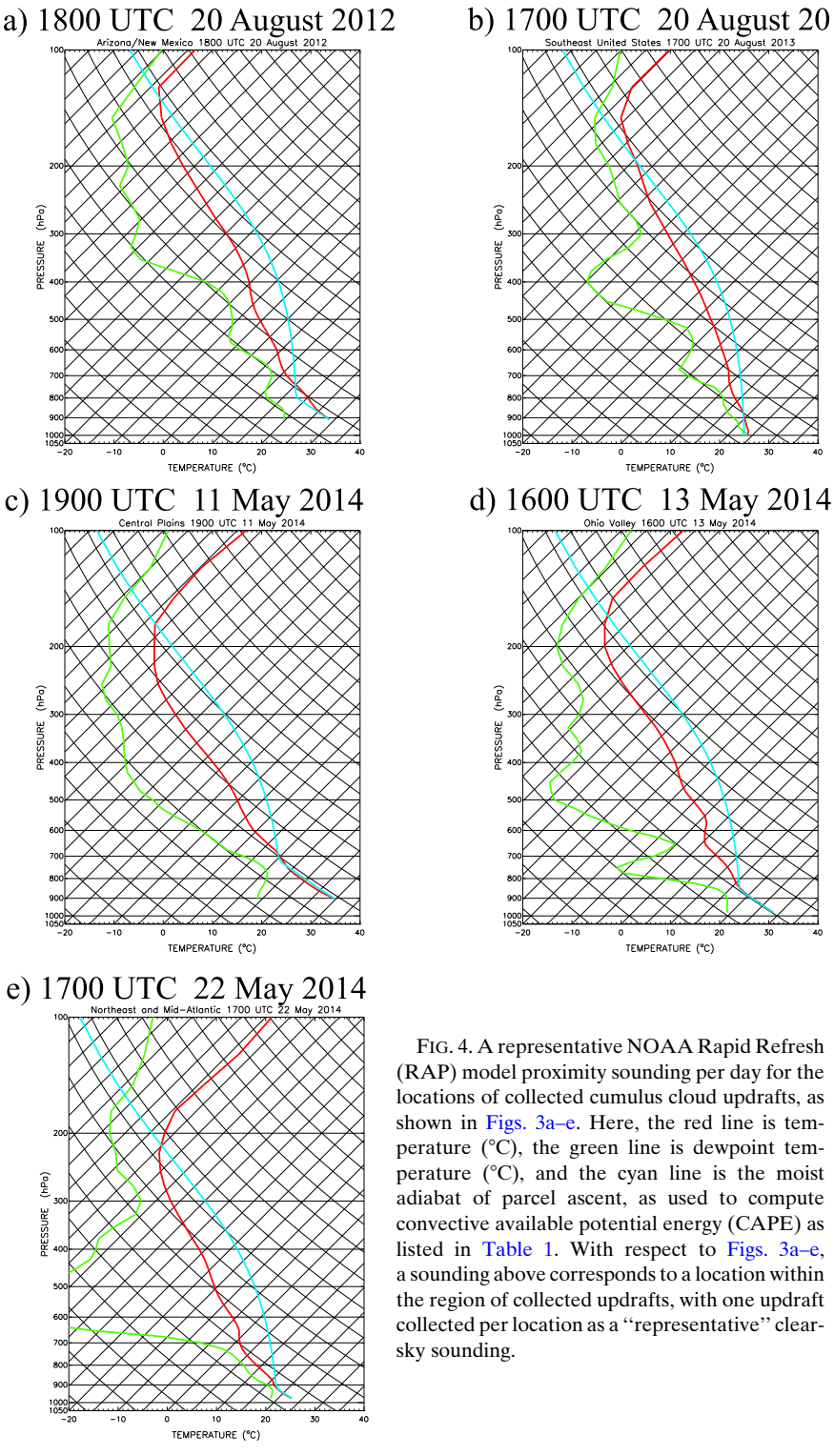

FIG. 4. A representative NOAA Rapid Refresh (RAP) model proximity sounding per day for the locations of collected cumulus cloud updrafts, as shown in Figs. 3a–e. Here, the red line is temperature (°C), the green line is dewpoint temperature (°C), and the cyan line is the moist adiabat of parcel ascent, as used to compute convective available potential energy (CAPE) as listed in Table 1. With respect to Figs. 3a–e, a sounding above corresponds to a location within the region of collected updrafts, with one updraft collected per location as a ''representative'' clear-sky sounding.

above ground level (AGL). Updrafts on 20 August 2013 (Fig. 2b) were first detected between 4200 and 6300 m AGL. Cloud-to-cloud growth characteristics in Figs. 2a and 2b varied considerably, yet for nearly all cases, a short period of very rapid vertical growth was generally observed, on the order of 2000–3500 m in ≤5 min when cloud-top temperatures were ≤250–260 K. This rapid growth signature may have been partly caused by

subpixel-sized cumulus clouds filling the GOES IR pixels, hence causing a rapid cooling (which was interpreted as increased updraft velocities). However, by the time the clouds reached these 250–260-K cloud-top temperatures and associated altitudes, they most often were larger than 4–6 km in diameter. Furthermore, the continuous cooling of the cloud top suggested that the overall cloud structure was building upward and had not yet reached the level of neutral buoyancy where horizontal expansion is the primary kinetic mode. Updrafts on 11 May 2014 (Fig. 2c) were collected for only six growing cumulus cloud cases, yet these clouds all later evolved into supercells and more organized-type convection storms, and showed very rapid growth in the first 40 min of data collection, to an approximate EL near 10 500–11 000 m AGL. In contrast to 11 May, updrafts on 13 and 22 May showed much more gradual growth rates, with more embedded rapid growth periods. Cloud development on 22 May was the most gradual of all days. It is important to note, along the lines of discussion in Lensky and Rosenfeld (2006), that since the real resolution of the *GOES-14* data at the latitudes of interest is ~5 km × 5 km (or even lower), the existence of the good correlations (>0.60) between the satellite-smoothed ascent rate of the convective clusters and the local CAPE [i.e. $\sum\delta(\text{CAPE})^{1/2}$] suggests there exists a fundamental relationship between satellite-observed rising rates and local (meso-γ to meso-β scale; 2.5 to ~250 km) instability relevant to the environment within which a cumulus cloud is growing. In other words, given that actual cumulus clouds are of scales ~1–2 km, even the averaging occurring across the GOES pixels appears to not be enough to diminish the observed high δw–$\sum\delta(\text{CAPE})^{1/2}$ correlations.

Table 1 lists the characteristics of the environment as obtained from the proximity or representative RAP model-sounding locations within two model grid cells of updraft collections for the datasets shown in Figs. 2a–e. From Figs. 2a–e, Figs. 4a–e, and Table 1, common and interesting aspects of the updrafts observed in SRSOR data include the following: 1) highly variable vertical growth rates, to the maximum observed 1-min w of 24.4 m s^{-1} (at 1921 UTC 11 May 2014); cases of variable growth are likely connected to cloud-top evaporation, or a bubbling of the updrafts, leading to a lower, warmer part of the cloud being observed. 2) The altitude of largest vertical cloud growth occurred above ~6700 m regardless of the day, and below the local EL. 3) Signatures of overshooting cloud tops appear centered on a "local" EL for a given region or day. 4) The T_B when $\text{ref}_{39} < 9\%$ averages between 258 and ~268 K, except on 11 May 2014. The low "glaciation temperatures" near 251 K as seen on 11 May 2014 are consistent with the strong updrafts observed, and follow the theory outlined by Rosenfeld et al. (2008) that positively correlated rapid cumulus cloud updraft growth, small cloud effective radii of cloud particles (and hence higher visible reflectance), and low glaciation temperatures (see also Lensky and Rosenfeld 2006).

Related to (1) above, use of a special 1800 UTC sounding taken at Dodge City, Kansas (DDC), on 11 May 2014, in contrast to a proximity RAP model sounding, shows that the peak w varied from ~18.3 to over 31.4 m s^{-1}, showing a dependence on whether the environmental temperature profile or temperature of an assumed parcel is used when determining w. It is encouraging then that the maximum SRSOR-estimated w (using the methodology of section 2a on this day) is within these bounds at 24.4 m s^{-1}, and also that use of RAP model proximity soundings provide comparable results to when actual soundings are used.

Several other conclusions can be drawn from Figs. 2a–e. 1) Rapid increases in vertical velocities occur above in height (or below in temperature) both the RAP model-determined 0°C isotherm level and the level of ref_{39}–10.7 T_B determined cloud-top glaciation, which emphasizes the degree to which the latent heat of freezing influences cloud growth in the mid- and upper troposphere [as denoted by the first three terms in (3), especially $0.61q_v$]; the average ΔT ZLVL − MDA values in Table 1 range from 11.5 to 23.3 K. It is noteworthy that similar signatures are seen in the three clouds analyzed in Cintineo et al. (2013, see their Figs. 6a,c,e). Rapid accelerations in cloud-top cooling uncharacteristic of the monotonic decrease in T_B prior to freezing suggest that convective updraft invigoration occurred after glaciation was detected. These rapid increases in updraft acceleration above the 0°C isotherm level also are related to the shape of the B profile, being wider at these altitudes compared to nearer the LFC (see Fig. 4). This topic will be addressed in a follow-on study using cloud-resolving model simulations. 2) Cloud anvil development is associated with lower δw–$\sum\delta(\text{CAPE})^{1/2}$ correlations (below 0.60, as shown in Fig. 6 per the plotting convention of Fig. 5) at low temperatures with an oscillation around an EL, yet as the maximum updrafts appear to occur somewhat below the EL, pure parcel theory is apparently not being realized to cloud top. In other words, near the EL, changes in updraft speed δw are not related to changes in $\delta(\text{CAPE})^{1/2}$, likely due to complex interactions of the parcels with their environment that SRSOR observations cannot specifically resolve, such as cloud-top entrainment and gravity wave breaking. Another reason for an observed updraft maximum below the EL is related to vertical

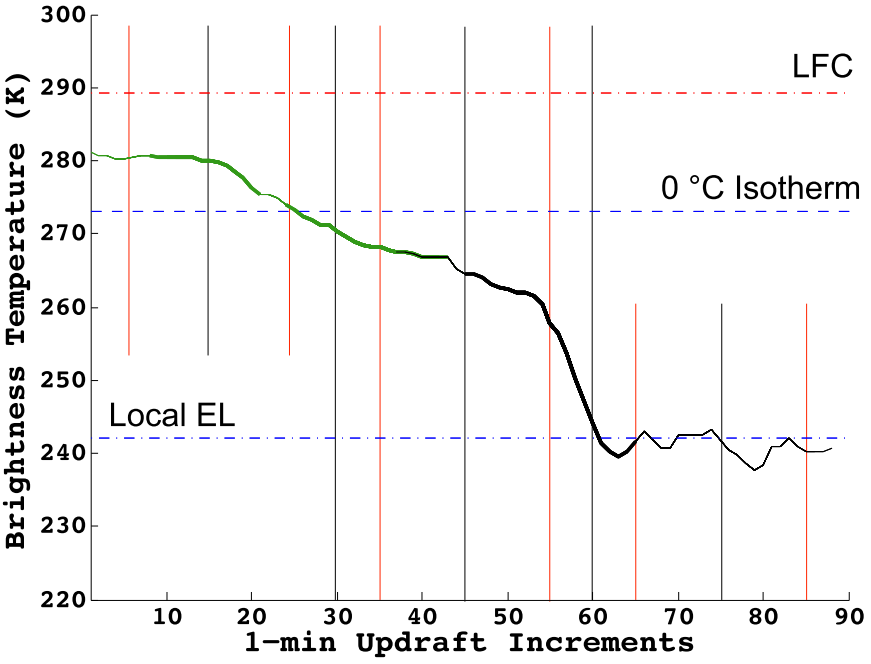

FIG. 5. Case example of a cumulus cloud updraft growing on 20 Aug 2012 between 1702 and 1830 UTC (0–87 min). The thin green line segments pertain to times when the incremental vertical motion (δw) was correlated with the summed convective available potential energy $(\delta\text{CAPE})^{1/2}$ [$\sum\delta$CAPE] at <0.60, while the thick green lines are time periods when these two quantities were correlated at ≥ 0.60. Black thin and thick lines follow the same convention, yet black signifies that the cumulus cloud has a cloud-top 3.9-μm reflectance $<9\%$, which implies cloud-top glaciation (see Lindsey et al. 2006). The vertical lines relate to even 15-min time intervals (to mimic the "operational" data resolution for GOES), while the red lines are shown at 05, 25, 35, and 55 min after the top of an hour (to mimic extra "rapid scan" data as collected by GOES). In this figure, "0" min on the x axis pertains to 1702 UTC, 10 min is 1712 UTC, etc. See text for description of updraft behavior.

perturbation high pressures forming at some distance below the EL/tropopause, causing an updraft to decelerate before reaching the EL/tropopause, as demonstrated in high-resolution cloud-resolving model simulations (Parker 2010; Morrison 2016). 3) Given the varying altitudes of anvil formation, influences of entrainment appear to be evident as parcels reach an EL in various states (i.e., more or less diluted with environmental air) and follow parcel theory to lesser degrees. It was found that the EL temperatures from SRSOR observations were warmer than those found from an unentrained parcel, or specifically, the clouds reached levels of neutral buoyancy prior to the point where parcel theory predicted where one would have been reached. Again, the use of other datasets is required to confirm this conjecture such as cloud-resolving modeling, photogrammetric analysis along with a cloud radar, and/or a parcel model on a case-by-case basis, yet past research shows similar findings (Reuter and Yau 1987). 4) In regions of the updraft where δw–$\sum\delta(\text{CAPE})^{1/2}$ correlations are >0.60 or as high as >0.80, it may be theoretically possible to use satellite data alone from one T_B channel (10.7 μm) and derive a B profile if only the values for δw are known based on (3).

Figure 5 shows how these SRSOR data can subsequently be displayed toward showing updraft characteristics, from near the LFC to when the 0°C isotherm level is reached, and with respect to when there is high confidence that the cloud tops have glaciated. In Fig. 5, one updraft that extended from 1702 (0 min) to 1830 UTC (87 min) on 20 August 2012 is shown, with the LFC, 0°C isotherm level, and local EL depicted, with time on the x axis and cloud-top temperature (K) on the y axis. Portions of the updraft in color (green) are bolded versus thin, which are times when the correlation between δw and the $\sum\delta(\text{CAPE})^{1/2}$ within the vertical layer the updraft moved through (in running 10-min segments) is ≥ 0.60 as described in section 2b. The bolded segment is shown to highlight where the updraft is strongly related to the instability within a portion of a sounding, or specifically to the amount of CAPE and perhaps the shape of the B profile. In other words, the

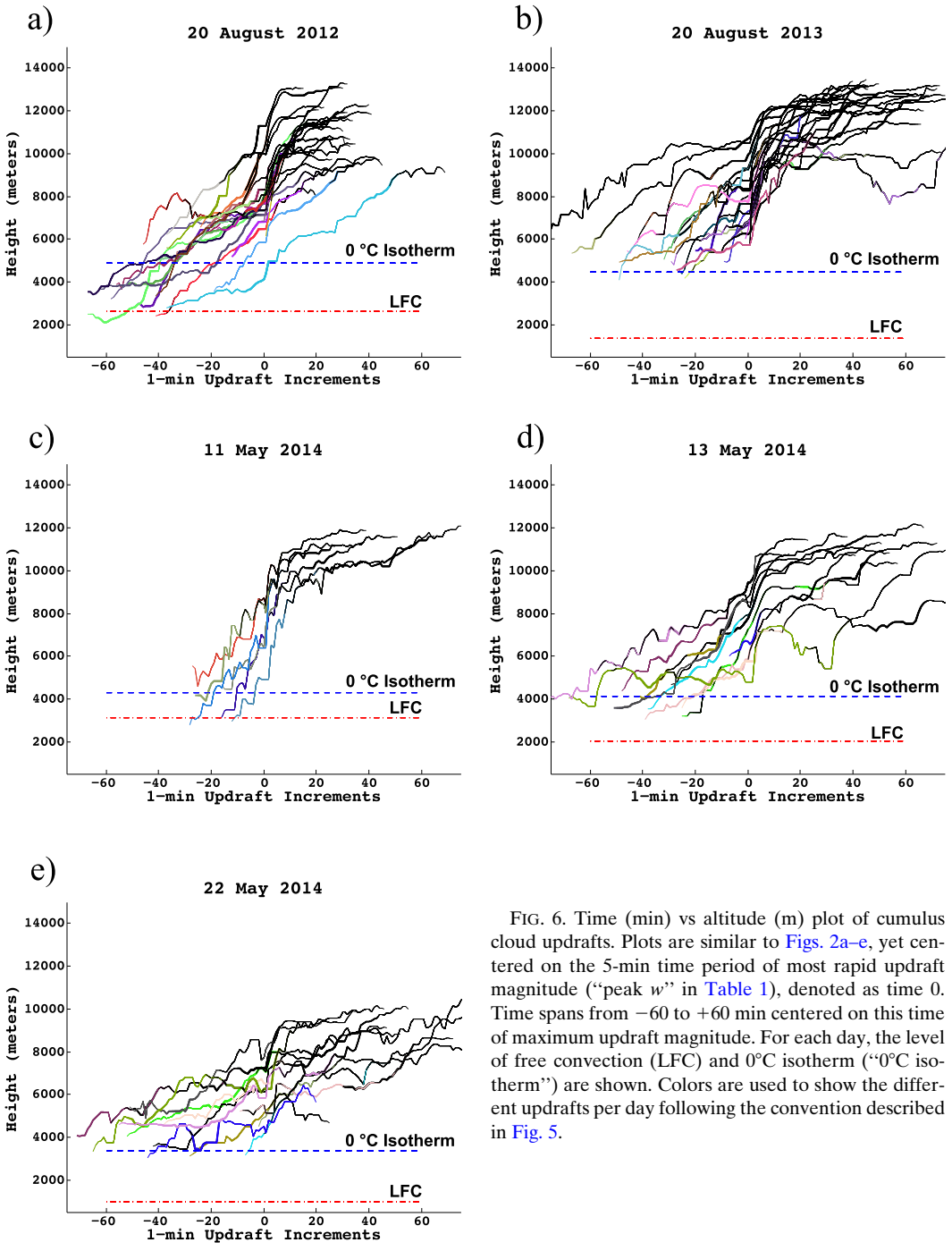

FIG. 6. Time (min) vs altitude (m) plot of cumulus cloud updrafts. Plots are similar to Figs. 2a–e, yet centered on the 5-min time period of most rapid updraft magnitude ("peak w" in Table 1), denoted as time 0. Time spans from −60 to +60 min centered on this time of maximum updraft magnitude. For each day, the level of free convection (LFC) and 0°C isotherm ("0°C isotherm") are shown. Colors are used to show the different updrafts per day following the convention described in Fig. 5.

bold line depicts where an increase in w is observed with an increase in CAPE (or vice versa). In this case on 20 August 2012, glaciation occurred after minute 40 of cloud development (the line became black in color), and the cloud's top remained glaciated through minute 87. This convention for plotting the updrafts is followed as all updrafts are analyzed in Fig. 6.

Also shown in Fig. 5 are black vertical lines every 15 min (the current operational GOES time resolution), and at more intermittent intervals in red (5, 25, 35, and 55 min after the hour) to show the current GOES "rapid scan" mode of data collection; these vertical lines are shown for comparison purposes and to demonstrate the improved information available at 1-min time resolution

data for rapidly changing phenomena like growing cumulus clouds. Note that the rapid growth period extending from ~53 and 62 min is smoothed considerably when only 15-min resolution data are available, and fortuitously in this event, more traditional rapid scan GOES would have reasonably well captured this rapid growth segment, which is not always the case.

Unlike Figs. 2a–e, data in Figs. 6a–c are plotted with the "0 time" being the time of maximum δw for each updraft. These plots serve to compare the updrafts by a common time of cloud development such that general behaviors can be measured across a population of events. The choice was made to normalize based on a maximum δw for each updraft versus the altitude of glaciation since not all updrafts exhibited obvious glaciation (as denoted by ref_{39} falling below 9%), and since cloud-top glaciation may not be strongly related to in-cloud glaciation. Note that for a few updrafts (shown by black-colored patterns), the cloud's top transitioned repeatedly from glaciated to unglaciated. For these clouds, the speculation is that as one cumulus cloud turret glaciated and weakened, a following turret or updraft penetrated through the 0°C isotherm level that was not glaciated initially, yet traveled upward and glaciated at a somewhat later time (by several minutes). It is particularly interesting that these more subtle features of cumulus cloud growth are observed in the 4-km resolution, 1-min data, which is quite different than what would be seen in the more typical 15-min GOES observations (recall Fig. 5 referencing current GOES data collection strategies).

b. *General statistical behaviors*

Figures 7a–f show the variability in the time evolution of updraft heights on all days, and then collectively (Fig. 7f), through the use of so-called box plots. As in Fig. 6, all updrafts on a given day were plotted with the 0 time at the time of maximum δw for each updraft to compare the updrafts by a common time of cloud development. Box plots were developed to show the median, 25% upper quartile, 75% lower quartile, maximum, minimum, and outlier values (as plus signs) in a compact form at 5-min time intervals for all updrafts that occurred per time period. The purpose of presenting the updraft data in this manner was to help identify the consistent features of updrafts across our population of events.

From Fig. 7, key signatures include a period of slower updraft growth in the −50 to −30 min period, a jump in updraft velocities centered on 0 min (the time of maximum δw) and generally at ~8000 m AGL, and an anvil/overshooting top signature with diminished vertical growth at some time after the period of maximum updraft strength and high updraft-to-updraft variability. Given the sizes of the 25th and 75th percent quartiles, updraft-to-updraft variability tended to be lower in the 30 min prior to peak updraft velocities on 20 August 2012 (Fig. 7a) and 13 May 2014 (Fig. 7d), yet was lower toward anvil formation beyond +30 min on 20 August 2013 (Fig. 7b). The generally slow nature of cumulus cloud development on 22 May 2014 (Fig. 7e), as dictated by the smaller slope to the box plot median values over time, is evident. The small sample size (six cases) on 11 May 2014 (Fig. 7c) only shows the very rapid growth of clouds as also seen in Fig. 6c, with little other statistical information able to be determined.

Relative to the absolute, bulk CAPE values (Table 1) and the RAP model profiles (Figs. 4a–e), some of the results in Figs. 7a–f are explained, while others are not. On 20 August 2012, a representative surface-based CAPE value for the convective clouds sampled was 2228 J kg^{-1}. Theoretical peak updraft velocities given the relationship $w_{\max} \sim \sqrt{2 \times \text{CAPE}}$ would be near 66.8 m s^{-1}, which is well known to be a large overestimate of actual updraft velocities, and that is much above the estimated updraft velocities, that remained below 22 m s^{-1}. The lower value of observed w is likely to be the result of entrainment of environmental air into the growing cumulus clouds, whose influences are challenging to directly measure from SRSOR observations and can only be inferred. Prior studies have confirmed that cloud rising rates are about 50% the core updraft magnitude within the cloud (Romps and Charn 2015). Since the w scales as CAPE, with all things being equal, cloud growth should have been most rapid on 13 May 2014, yet this was not the case. An additional analysis of the soundings shows that the 13 May and 22 May cases both had large dry air layers aloft along with elevated stable layers, which when entrained into the parcel act to decrease the cloud's B more so than the August cases in which higher dewpoint values prevailed throughout the depth of the troposphere. Enhanced entrainment effects are apparent in the 13 May and 22 May cases, at least upon initial ascent, as cloud-top cooling exhibits a slow, stepped monotonic increase as the convective complexes frequently reached levels of neutral B along upward traverse. The slow, monotonic increase of the high CAPE case on 13 May 2014 suggests that parcel entrainment could cause a significant problem with the utility of cloud-top cooling-based severe thunderstorm nowcasting algorithms, which rely on the initial ascent of a parcel to characterize the updraft characteristics for the forthcoming storm.

Other results from this study that demand additional analyses using nonsatellite datasets (radar, cloud-resolving models) along with SRSOR data, include the following: 1) Updrafts were observed to grow quickest

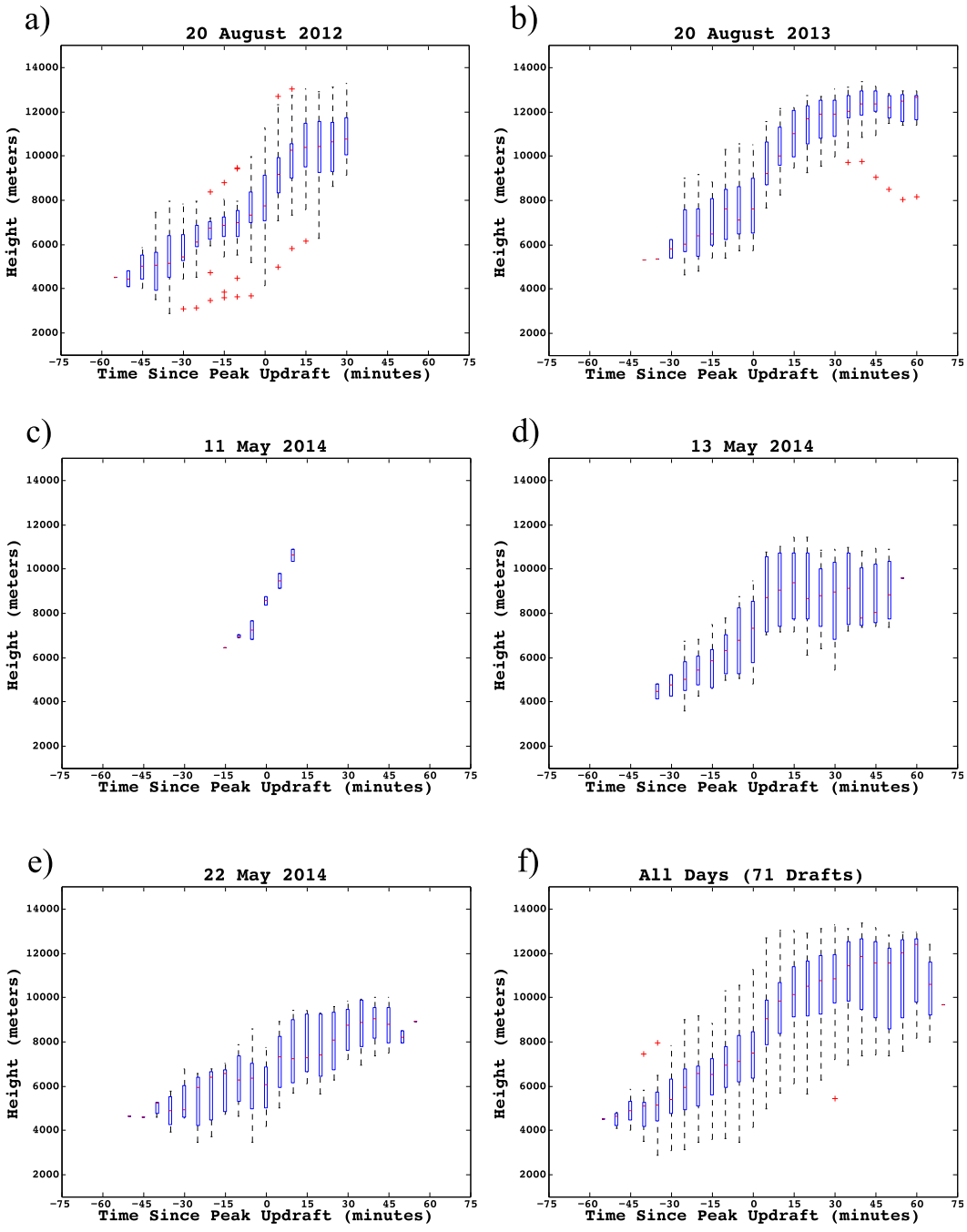

FIG. 7. (a)–(e) Box plots of all updrafts on a given day. Time spans from −75 to +75 min of updraft growth, with 0 min being the time of maximum vertical motion (as in Fig. 6), while height is shown in meters from 1000 to 15 000. (f) All days combined. Box plots follow the convention of the median value (red line) separating the 25% and 75% quartile ranges, with outliers shown as red crosses.

on 11 May 2014 while CAPE values were not the highest overall. 2) CAPE values were larger on 22 May 2014, yet the clouds were seen to grow at slower rates as compared to those on 11 May 2014. 3) On 12 August 2013, with representative bulk surface-based CAPE values only near 1500 J kg^{-1}, updrafts appeared to grow as rapidly as on 13 May, and much more rapidly than on 22 May, suggesting again that entrainment of environmental air into growing cumulus clouds changed the CAPE–w relationship. These discrepancies may be somewhat

related to uncertainties in our methods for retrieving w from cloud-top T_B changes versus analyzing updrafts within clouds, and yet they are also likely related to physical factors in the near-storm environment such as wind shear [acting to organize the convective updrafts, allowing them to more efficiently use the available CAPE; McCaul and Weisman (2001); Sherburn and Parker (2014)], and/or entrainment rates of dry environmental air that weakens updrafts (Marwitz 1973), especially when CAPE is $<3500\,\mathrm{J\,kg^{-1}}$ (James and Markowski 2010) as was the case in this study's dataset.

From Table 1, average values of several parameters are shown for each of the five days analyzed. For the population of events, updrafts reach maximum velocity above 6700 m AGL, which is from 3233 to 4304 m above the 0°C isotherm level for all five days. The MDA altitudes were on average ~12–23 K cooler than the 0°C isotherm level. For 22 May, the day with the strongest updrafts, the updrafts peaked in velocity closer to the 0°C isotherm level (surface-based CAPE values near $2590\,\mathrm{J\,kg^{-1}}$), while on 20 August 2013, the updrafts peaked (on average) ~4300 m above the 0°C isotherm altitude, despite the surface-based CAPE values only being near $1500\,\mathrm{J\,kg^{-1}}$. The strong updraft signature on 22 May could have been influenced to some degree by small initial clouds filling pixels over time, especially early within a cloud growth (before ~20 min), leading to enhanced cloud-top cooling rates and subsequently interpreted as high w values. In short, from the data in Table 1 for the population of updrafts analyzed, there are consistent relationships between the MDA relative to the 0°C isotherm level, while almost no relationships are found between mean initial updraft velocities and the bulk CAPE values. These weak relationships to bulk CAPE values suggest then that other processes are involved that influence overall initial updraft magnitude, such as entrainment.

For the complete 71-updraft population (Fig. 7f), more smoothed-out signatures are seen. Specifically, generally low population variability about the median occurs from −50 to 0 min, with a sharp jump in updraft velocity seen between 0 and +10 min, with a gradual increase in variability occurring after +10 min. This increase in variability beyond +10 min reflects the varying rates of anvil development and the occurrences of penetrative overshooting cloud tops across our dataset. On more explosive growth events, larger overshooting tops occurred (as seen well on 20 August 2012; Fig. 5), while on other days, anvil development, or clouds reaching a local EL, occurred over a wider time range relative to the MDA time (0 min). It is suggested that the jump in updraft velocity occurs in association with the glaciation of cloud top as parcels are warmed by the release of latent heat due to hydrometeor freezing, in association with the general widening of the B profile above the 0°C isotherm.

4. Discussion

The varying behaviors seen across a population of updrafts are unique as SRSOR observations measure rapidly growing cumulus clouds over several days in this small dataset. However, as noted above, there remains questions as to what in-cloud and stability-related processes are in fact being observed, versus what may be artifacts of the data themselves related to the inherent smoothing that occurs across 4-km IR resolution pixels. In particular, varying acceleration rates, which occur across large numbers of updrafts, along with noted periods of acceleration with respect to the 0°C isotherm level, appear to be robust features within this dataset. From (2), scale analysis shows that the largest factor influencing dw/dt is parcel instability (the first three terms). Therefore, the SRSOR-observed updraft (dw/dt) data should show the strongest relationships to CAPE and the B profile when entrainment and other factors have minimal impact on the vertical evolution of the storm.

Zipser (2003) references the behavior of cumulus cloud updrafts with respect to "hot towers" within the deep tropics. Related to studies by Johnson and Kriete (1982), Ooyama (1990), Johnson et al. (1999), and Cotton et al. (2011, p. 327), it is well accepted that the glaciation process reinvigorates convective updrafts at altitudes above the 0°C isotherm level. Glaciation in cumulus clouds occurs over a wide range of temperatures, from −5° to −15°C in tropical oceanic environments (Zipser 2003) to near the homogenous freezing point in severe convective storms over land (near −38°C). Relevant to the present study, the increase in updrafts observed at some distance above the 0°C isotherm level (Fig. 2) would seem to relate well with these prior observational studies. It should be noted that from Figs. 4a–e, the B profiles (T_v values) tend to be widest (largest) in the middle troposphere (above the 0°C isotherm level), which also supports increased updraft acceleration at these altitudes (McCaul and Weisman 2001). Data in Table 1 show that cloud growth rates (the MDA) peak in the temperature range from 12 to 23 K below the 0°C isotherm level. It must be noted that the actual cloud-top temperature is colder that those values estimated from *GOES-14* because the coldest tops are smeared by the low, ~4-km resolution. Assuming that some period of time elapsed before the latent heating over the cloud (in-cloud hydrometeors upward to cloud top) was realized as updraft acceleration, these MDA

values fall roughly midway between tropical and severe convective updrafts, as found in the studies above. It must be noted that there is not necessarily a close correspondence between cloud-top glaciation, as inferred from ref_{39} and 10.7-μm T_B SRSOR data, and in-cloud hydrometeor glaciation that occurs deeper within the less diluted updraft core of a maturing cumulus cloud. Therefore, to fully confirm these conclusions high-resolution (100–500 m) cloud-resolving modeling, cloud radar hydrometeor characterization, and/or coincident aircraft observational analysis would need to be performed for SRSOR-observed cumulus clouds. It was found (Table 1) that the T_B when ref_{39} fell below 9% was coldest when SRSOR updrafts were strongest, which is consistent with prior studies by Rosenfeld and Woodley (2000), Lensky and Rosenfeld (2006), and Rosenfeld et al. (2008).

Another related interpretation of the updraft acceleration data discussed here is that some time is required for the subcloud base mesoscale (meso-γ scale; 2.5–25 km or larger) flows to form that subsequently support deeper cumulus cloud updraft development and maturation into the middle troposphere. From Figs. 6a–e, the time for updrafts to begin accelerating more rapidly at altitudes above the 0°C isotherm level is 20 to sometimes >60 min after the cloud extends above the LFC (i.e., the period of slower growth), which is consistent with the advanced lead times that satellite data provide when nowcasting convective initiation (Roberts and Rutledge 2003; Mecikalski and Bedka 2006; Walker et al. 2012). Along the lines of Ziegler and Rasmussen (1998), Peckham et al. (2004), and Buban et al. (2007), the ''convective initiation process'' is inherently connected to the organization of three-dimensional boundary layer flows that ultimately support deeper convective storm development, which take some amount of time to form beyond the time that a cumulus cloud first extends above the LFC.

Given that entrainment and to some extent influences related to dynamical, nonhydrostatic (pressure perturbation) forces were influencing the rates of acceleration of the SRSOR observed cumulus clouds, it is felt that there is not enough information within only the *GOES-14* data to more precisely quantify the entrainment process. It is clear, based on the varying altitudes of the cloud tops, or local EL, that some updrafts were less diluted upon initial ascent than others. Also, the varying relationships between cloud growth rates versus CAPE as seen on 11 May in contrast with 22 May 2014 exemplify influences of entrainment and likely nonhydrostatic influences on cloud development. Again, the use of cloud radar observations, cloud-resolving model simulations, and/or photogrammetric datasets would be needed to corroborate the SRSOR dataset, which is the goal of future analysis.

5. Conclusions

A study was undertaken to assess the general characteristics of cumulus cloud growth rates as observed in 1-min time resolution SRSOR observations, as collected for select dates and locations by *GOES-14* during the warm seasons of 2012–15. These SRSOR observations are available on time scales appropriate when characterizing rapidly changing atmospheric phenomenon, in this case, growing convective clouds in advance of thunderstorm formation. A total of 71 separate cumulus clouds were tracked for periods of 33–152 min.

The main conclusions from this study are as follows:

(i) The 1-min time resolution details of cumulus cloud updrafts reveal short-term (~2–5 min) fluctuations in updraft velocity, acceleration, and glaciation (occasionally alternating between glaciated tops, to unglaciated, as new updrafts penetrate a local EL; e.g., Fig. 2d). Cloud-top glaciation is estimated as the time when the *GOES-14* ref_{39} falls below 9% or when the 10.7-μm T_B fell to 235 K (−38°C) or below.

(ii) Clear signatures of anvil formation and overshooting cloud tops are seen in individual updrafts (e.g., in Fig. 5 and on 11 May 2014 in Fig. 6c).

(iii) Rapid increases in updraft strength are seen within 5–10 min after clouds glaciate, with the MDA varying from 6788 to 8784 m AGL as an average per day. The conclusion is that the added latent heat from the glaciation process invigorates updrafts, along the lines of prior studies, which is observed in these SRSOR data. Glaciation of cloud top as estimated in SRSOR data is suggested as indicating the glaciation of in-cloud hydrometeors, which, however, will require further analysis to confirm (using WSR-88DP radar and cloud-resolving models). These rapid increases in updrafts also are related to the B profile being widest in the middle troposphere in general for most days analyzed, as seen in the RAP model proximity soundings in Figs. 4a–e.

(iv) From the independent datasets of SRSOR-estimated w and RAP model B profiles, segments of many updrafts showed high correlation (>0.60 to more than 0.80) between per layer w (δw) and accumulated per layer CAPE [$\delta(\text{CAPE})^{1/2}$] values, $\sum\delta(\text{CAPE})^{1/2}$. Here, ''per layer'' is the layer of air an updraft moved through in 1 min, which is related to a portion of the entire B profile.

This study is viewed as a first-level analysis of these unique SRSOR observations for rapidly evolving convective clouds. To corroborate further presumed signals in 1-min data of processes such as entrainment, the overall instability, the shape of the *B* profile, and overshooting top structures, additional analysis would be needed involving nonsatellite observations. Specifically, dual-Doppler and radar analysis for an SRSOR-observed growing cumulus cloud (that grows into a convective storm) would help complete the picture on how GOES-observed updrafts relate to radar-measured updraft velocities and volumes, as well as to the development of in-cloud hydrometeor fields. Comparisons between SRSOR-observed clouds and photogrammetric observations would also be an important way to confirm the updraft characteristics listed in Table 1. Valuable information would also come from high-resolution (sub 1 km) cloud-resolving model simulations of the convection that form in the environments in which SRSOR observations are collected (as done in Houston and Niyogi 2007). Model output could be analyzed to quantify aspects on how the ambient flow, stability, and moisture distributions affect cloud organization, internal pressure fields, and growth rates, which are subsequently influenced by entrainment and hydrometeor distributions (i.e., latent heating). A combined satellite–radar–modeling study, therefore, would be a future plan.

The uses of RAP model soundings (vs radiosonde data) may be contributing to the following issues: problems of representativeness between a model-based parcel and parcels that actually produce the observed clouds, model biases, and incorrect model analyses. For example, the RAP model used at the time of this study had a high bias in the tropopause altitude, and hence in the EL and CAPE values (S. Weygandt, NOAA, 2013, personal communication), which needs to be considered in the analysis to follow. Despite these known problems, the RAP model is one of the better ways to approximate thermodynamic variables in a changing three-dimensional environment without sounding data, enough to make some quantitative conclusions.

Cloud-top entrainment may cause problems with the temperature height assignment when assuming that a parcel has conserved values of equivalent potential temperature throughout its ascent. Also, the release of latent heat by freezing hydrometeors will affect the temperature profiles of clouds in a way that currently cannot be captured by the *w*-estimation methodology used in this study. The presented methodology for analyzing the growth of individual clouds assumed that cloud tracking was done correctly, and that a 16 km^2 IR pixel provided a representative temperature value for the top of the updraft, while in actuality, cumulus cloud tops were likely colder given the smoothing of sub-4-km-scale updraft turrets. While the current study makes the assumption that the updraft as a whole behaves in a way that is predictable by (3), use of higher spatial resolution datasets, such as the 2-km IR set to be available upon the launch of GOES-R, may act to reduce the warm bias introduced by the oversmoothing of current *GOES-14* channels.

Finally, given that SRSOR observations will become common in the GOES-R era (late 2016 and beyond), and that these observations are at time frequencies more consistent with WSR-88DP radar, the meteorological community will be challenged to more integrated use of 30-s to 1-min resolution satellite data in the weather forecasting, and warning decision process. A sound path forward will involve integrating SRSOR observations and short-term prediction products derived from these data into real-time advanced warning tools, such as Warn-on-Forecast (Stensrud et al. 2009), and Forecasting a Continuum of Environmental Threats (FACETs) as part of Weather Ready Nation (Lindell and Brooks 2013).

Acknowledgments. This research was funded by National Science Foundation Grant AGS–1261386 and National Oceanic and Atmospheric Administration Award NA11NES4400014. The authors thank Dr. Dan Lindsey for help acquiring the 1-min resolution *GOES-14* data used in this study. We also want to thank four anonymous reviewers for helping to significantly improve the quality of this manuscript.

REFERENCES

Adler, R. F., and D. D. Fenn, 1979: Thunderstorm vertical velocities estimated from satellite data. *J. Atmos. Sci.*, **36**, 1747–1754, doi:10.1175/1520-0469(1979)036<1747:TVVEFS>2.0.CO;2.

——, and ——, 1981: Satellite-observed cloud-top height changes in tornadic thunderstorms. *J. Appl. Meteor.*, **20**, 1369–1375, doi:10.1175/1520-0450(1981)020<1369:SOCTHC>2.0.CO;2.

Barnes, G. M., 1995: Updraft evolution: A perspective from cloud base. *Mon. Wea. Rev.*, **123**, 2693–2715, doi:10.1175/1520-0493(1995)123<2693:UEAPFC>2.0.CO;2.

Baum, B. A., P. F. Soulen, K. I. Strabala, M. D. King, S. A. Ackerman, W. P. Menzel, and P. Yang, 2000: Remote sensing of cloud properties using MODIS airborne simulator imagery during SUCCESS. 2. Cloud thermodynamic phase. *J. Geophys. Res.*, **105**, 11 781–11 792, doi:10.1029/1999JD901090.

Bedka, K., J. Brunner, R. Dworak, W. Feltz, J. Otkin, and T. Greenwald, 2010: Objective satellite-based detection of overshooting tops using infrared window channel brightness temperature gradients. *J. Appl. Meteor. Climatol.*, **49**, 181–202, doi:10.1175/2009JAMC2286.1.

——, R. Dworak, J. Brunner, and W. Feltz, 2012: Validation of satellite-based objective overshooting cloud-top detection methods using *CloudSat* cloud profiling radar observations. *J. Appl. Meteor. Climatol.*, **51**, 1811–1822, doi:10.1175/JAMC-D-11-0131.1.

Benjamin, S. G., and Coauthors, 2009: Rapid Refresh/Rapid Update Cycle (RR/RUC) technical review. NOAA/ESRL/GSD Internal Review, 168 pp. [Available online at http://ruc.noaa.gov/pdf/RR-RUC-TR_11_3_2009.pdf.]

Bonesteele, R. G., and Y. J. Lin, 1978: A study of updraft–downdraft interaction based on perturbation pressure and single-Doppler radar data. *Mon. Wea. Rev.*, **106**, 62–68, doi:10.1175/1520-0493(1978)106<0062:ASOUDI>2.0.CO;2.

Buban, M. S., C. L. Ziegler, E. N. Rasmussen, and Y. P. Richardson, 2007: The dryline on 22 May 2002 during IHOP: Ground-radar and in situ data analyses of the dryline and boundary layer evolution. *Mon. Wea. Rev.*, **135**, 2473–2505, doi:10.1175/MWR3453.1.

Byers, H. R., and R. R. Braham, 1949: *The Thunderstorm*. U.S. Dept. of Commerce, 287 pp.

Cho, H.-R., 1985: Rates of entrainment and detrainment of momentum of cumulus clouds. *Mon. Wea. Rev.*, **113**, 1920–1932, doi:10.1175/1520-0493(1985)113<1920:ROEADO>2.0.CO;2.

Cintineo, J. L., M. J. Pavolonis, J. M. Sieglaff, and A. K. Heidinger, 2013: Evolution of severe and nonsevere convection inferred from GOES-derived cloud properties. *J. Appl. Meteor. Climatol.*, **52**, 2009–2023, doi:10.1175/JAMC-D-12-0330.1.

Cohen, J., P. Cohen, S. G. West, and L. S. Aiken, 2003: *Applied Multiple Regression/Correlation Analysis for the Behavioral Sciences.* 3rd ed. Routledge, 736 pp.

Cotton, W. R., G. H. Bryan, and S. C. van den Heever, 2011: *Storm and Cloud Dynamics—The Dynamics of Clouds and Precipitating Mesoscale Systems.* 2nd ed. Academic Press, 809 pp.

Doswell, C. A., III, and P. M. Markowski, 2004: Is buoyancy a relative quantity? *Mon. Wea. Rev.*, **132**, 853–863, doi:10.1175/1520-0493(2004)132<0853:IBARQ>2.0.CO;2.

Emanuel, K. A., 1994: *Atmospheric Convection*. Oxford University Press, 580 pp.

Geerts, B., T. Andretta, S. J. Luberda, J. Vogt, Y. Wang, L. D. Oolman, J. Finch, and D. Bikos, 2009: A case study of a long-lived tornadic mesocyclone in a low-CAPE complex-terrain environment. *Electron. J. Severe Storms Meteor*, **4** (3), 1–29. [Available online at http://www.ejssm.org/ojs/index.php/ejssm/article/viewArticle/59.]

Goodman, S. J., and Coauthors, 2012: The GOES-R Proving Ground: Accelerating user readiness for the next-generation geostationary environmental satellite system. *Bull. Amer. Meteor. Soc.*, **93**, 1029–1040, doi:10.1175/BAMS-D-11-00175.1.

Hong, G., P. Yang, B.-C. Gao, B. A. Baum, Y. X. Hu, M. D. King, and S. Platnick, 2007: High cloud properties from three years of MODIS *Terra* and *Aqua* collection-4 data over the tropics. *J. Appl. Meteor. Climatol.*, **46**, 1840–1856, doi:10.1175/2007JAMC1583.1.

Houston, A. L., and D. Niyogi, 2007: The sensitivity of convective initiation to the lapse rate of the active cloud-bearing layer. *Mon. Wea. Rev.*, **135**, 3013–3032, doi:10.1175/MWR3449.1.

Houze, R. A., Jr., 1993: *Cloud Dynamics.* Academic Press, 573 pp.

James, R. P., and P. M. Markowski, 2010: A numerical investigation of the effects of dry air aloft on deep convection. *Mon. Wea. Rev.*, **138**, 140–161, doi:10.1175/2009MWR3018.1.

Johnson, R. H., and D. C. Kriete, 1982: Thermodynamic and circulation characteristics, of winter monsoon tropical mesoscale convection. *Mon. Wea. Rev.*, **110**, 1898–1911, doi:10.1175/1520-0493(1982)110<1898:TACCOW>2.0.CO;2.

——, T. M. Rickenbach, S. A. Rutledge, P. E. Ciesielski, and W. H. Schubert, 1999: Trimodal characteristics of tropical convection. *J. Climate*, **12**, 2397–2418, doi:10.1175/1520-0442(1999)012<2397:TCOTC>2.0.CO;2.

Kirkpatrick, C., E. W. McCaul Jr., and C. Cohen, 2011: Sensitivities of simulated convective storms to environmental CAPE. *Mon. Wea. Rev.*, **139**, 3514–3532, doi:10.1175/2011MWR3631.1.

Lensky, I. M., and D. Rosenfeld, 2006: The time-space exchangeability of satellite retrieved relations between cloud top temperature and particle effective radius. *Atmos. Chem. Phys.*, **6**, 2887–2894, doi:10.5194/acp-6-2887-2006.

Lindell, M. K., and H. Brooks, 2013: Workshop on Weather Ready Nation: Science imperatives for severe thunderstorm research. *Bull. Amer. Meteor. Soc.*, **94**, ES171–ES174, doi:10.1175/BAMS-D-12-00238.1.

Lindsey, D. T., D. W. Hillger, L. Grasso, J. A. Knaff, and J. F. Dostalek, 2006: GOES climatology and analysis of thunderstorms with enhanced 3.9-μm reflectivity. *Mon. Wea. Rev.*, **134**, 2342–2353, doi:10.1175/MWR3211.1.

Ludlam, F. H., and R. S. Scorer, 1953: Convection in the atmosphere. *Quart. J. Roy. Meteor. Soc.*, **79**, 317–341, doi:10.1002/qj.49707934102.

Manzato, A., S. Davolio, M. M. Miglietta, A. Pucillo, and M. Setvák, 2015: 12 September 2012: A supercell outbreak in NE Italy? *Atmos. Res.*, **153**, 98–118, doi:10.1016/j.atmosres.2014.07.019.

Marwitz, J. D., 1973: Trajectories within the weak echo regions of hailstorms. *J. Appl. Meteor.*, **12**, 1174–1182, doi:10.1175/1520-0450(1973)012<1174:TWTWER>2.0.CO;2.

McCaul, E. W., Jr., and M. L. Weisman, 2001: The sensitivity of simulated supercell structure and intensity to variations in the shapes of environmental buoyancy and shear profiles. *Mon. Wea. Rev.*, **129**, 664–687, doi:10.1175/1520-0493(2001)129<0664:TSOSSS>2.0.CO;2.

Mecikalski, J. R., and K. M. Bedka, 2006: Forecasting convective initiation by monitoring the evolution of moving convection in daytime GOES imagery. *Mon. Wea. Rev.*, **134**, 49–78, doi:10.1175/MWR3062.1.

——, ——, S. J. Paech, and L. A. Litten, 2008: A statistical evaluation of GOES cloud-top properties for predicting convective initiation. *Mon. Wea. Rev.*, **136**, 4899–4914, doi:10.1175/2008MWR2352.1.

——, P. Watts, and M. Koenig, 2011: Use of Meteosat Second Generation Optimal Cloud Analysis fields for understanding physical attributes of growing cumulus clouds. *Atmos. Res.*, **102**, 175–19, doi:10.1016/j.atmosres.2011.06.023.

——, J. K. Williams, C. P. Jewett, D. Ahijevych, A. LeRoy, and J. R. Walker, 2015: Probabilistic 0–1-h convective initiation nowcasts that combine geostationary satellite observations and numerical weather prediction model data. *J. Appl. Meteor. Climatol.*, **54**, 1039–1059, doi:10.1175/JAMC-D-14-0129.1.

Min, Q., and M. Duan, 2005: Simultaneously retrieving cloud optical depth and effective radius for optically thin clouds. *J. Geophys. Res.*, **110**, D21201, doi:10.1029/2005JD006136.

Morrison, H., 2016: Impacts of updraft size and dimensionality on the perturbation pressure and vertical velocity in cumulus convection. Part II: Comparison of theoretical and numerical solutions and fully dynamical simulations. *J. Atmos. Sci.*, doi:10.1175/JAS-D-15-0041.1, in press.

Ooyama, K. V., 1990: A thermodynamic foundation for modeling the moist atmosphere. *J. Atmos. Sci.*, **47**, 2580–2593, doi:10.1175/1520-0469(1990)047<2580:ATFFMT>2.0.CO;2.

Parker, M. D., 2010: Relationship between system slope and updraft intensity in squall lines. *Mon. Wea. Rev.*, **138**, 3572–3578, doi:10.1175/2010MWR3441.1.

Peckham, A. E., R. B. Wilhelmson, L. J. Wicker, and C. L. Ziegler, 2004: Numerical simulation of the interaction between the dryline and horizontal convective rolls. *Mon. Wea.*

Rev., **132**, 1792–1812, doi:10.1175/1520-0493(2004)132<1792:NSOTIB>2.0.CO;2.

Reuter, G. W., and M. K. Yau, 1987: Mixing mechanisms in cumulus congestus clouds. Part I: Observations. *J. Atmos. Sci.*, **44**, 781–797, doi:10.1175/1520-0469(1987)044<0781:MMICCC>2.0.CO;2.

Roberts, R. D., and S. Rutledge, 2003: Nowcasting storm initiation and growth using *GOES-8* and WSR-88D data. *Wea. Forecasting*, **18**, 562–584, doi:10.1175/1520-0434(2003)018<0562:NSIAGU>2.0.CO;2.

Romps, D. M., and A. B. Charn, 2015: Sticky thermals: Evidence for a dominant balance between buoyancy and drag in cloud updrafts. *J. Atmos. Sci.*, **72**, 2890–2901, doi:10.1175/JAS-D-15-0042.1.

Rosenfeld, D., and W. L. Woodley, 2000: Deep convective clouds with sustained supercooled liquid water down to −37.5°C. *Nature*, **405**, 440–442, doi:10.1038/35013030.

——, ——, A. Lerner, G. Kelman, and D. T. Lindsey, 2008: Satellite detection of severe convective storms by their retrieved vertical profiles of cloud particle effective radius and thermodynamic phase. *J. Geophys. Res.*, **113**, D04208, doi:10.1029/2007JD008600.

Schmit, T. J., and Coauthors, 2015: Rapid refresh information of significant events: Preparing users for the next generation of geostationary operational satellites. *Bull. Amer. Meteor. Soc.*, **96**, 561–576, doi:10.1175/BAMS-D-13-00210.1.

Setvák, M., and J. Müller, 2013: MSG-3 Super Rapid Scan study. EUM/STG-SWG/34/13/DOC/06 (internal EUMETSAT document).

——, K. Bedka, D. T. Lindsey, A. Sokol, Z. Charvát, J. Šťástka, and P. K. Wang, 2013: A-Train observations of deep convective storm tops. *Atmos. Res.*, **123**, 229–248, doi:10.1016/j.atmosres.2012.06.020.

Sherburn, K. D., and M. D. Parker, 2014: Climatology and ingredients of significant severe convection in high shear, low CAPE environments. *Wea. Forecasting*, **29**, 854–877, doi:10.1175/WAF-D-13-00041.1.

Sieglaff, J. M., L. M. Cronce, W. F. Feltz, K. M. Bedka, M. J. Pavolonis, and A. K. Heidinger, 2011: Nowcasting convective storm initiation using satellite-based box-averaged cloud-top cooling and cloud-type trends. *J. Appl. Meteor. Climatol.*, **50**, 110–126, doi:10.1175/2010JAMC2496.1.

Sloss, P. W., 1967: An empirical examination of cumulus entrainment. *J. Appl. Meteor.*, **6**, 878–881, doi:10.1175/1520-0450(1967)006<0878:AEEOCE>2.0.CO;2.

Soper, D. S., 2015: p-value calculator for correlation coefficients. [Available online at http://www.danielsoper.com/statcalc.]

Stechmann, S. N., and B. Stevens, 2010: Multiscale models for cumulus cloud dynamics. *J. Atmos. Sci.*, **67**, 3269–3285, doi:10.1175/2010JAS3380.1.

Stensrud, D. J., and Coauthors, 2009: Convective-scale warn-on-forecast system: A vision for 2020. *Bull. Amer. Meteor. Soc.*, **90**, 1487–1499, doi:10.1175/2009BAMS2795.1.

Strabala, K. I., S. A. Ackerman, and W. P. Menzel, 1994: Cloud properties inferred from 8–12-μm data. *J. Appl. Meteor.*, **33**, 212–229, doi:10.1175/1520-0450(1994)033<0212:CPIFD>2.0.CO;2.

Walker, J. R., W. M. MacKenzie, J. R. Mecikalski, and C. P. Jewett, 2012: An enhanced geostationary satellite-based convective initiation algorithm for 0–2-h nowcasting with object tracking. *J. Appl. Meteor. Climatol.*, **51**, 1931–1949, doi:10.1175/JAMC-D-11-0246.1.

Weisman, M. L., and J. B. Klemp, 1982: The dependence of numerically simulated convective storms on vertical wind shear and buoyancy. *Mon. Wea. Rev.*, **110**, 504–520, doi:10.1175/1520-0493(1982)110<0504:TDONSC>2.0.CO;2.

Young, A. H., J. J. Bates, and J. A. Curry, 2012: Complementary use of passive and active remote sensing for detection of penetrating convection from CloudSat, CALIPSO, and Aqua MODIS. *J. Geophys. Res.*, **117**, D13205, doi:10.1029/2011JD016749.

Ziegler, C. L., and E. N. Rasmussen, 1998: The initiation of moist convection at the dryline: Forecasting issues from a case study perspective. *Wea. Forecasting*, **13**, 1106–1131, doi:10.1175/1520-0434(1998)013<1106:TIOMCA>2.0.CO;2.

Zipser, E. J., 2003: Some views on "hot towers" after 50 years of tropical field programs and two years of TRMM data. *Cloud Systems, Hurricanes, and the Tropical Rainfall Measuring Mission (TRMM)—A Tribute to Dr. Joanne Simpson, Meteor. Monogr.*, No. 51, Amer. Meteor. Soc., 49–58.